



OPEN

A magnetically retrievable mixed-valent $\text{Fe}_3\text{O}_4@\text{SiO}_2/\text{Pd}^0/\text{Pd}^{\text{II}}$ nanocomposite exhibiting facile tandem Suzuki coupling/transfer hydrogenation reaction

Parminder Singh^{1,2}, Saumyaranjan Mishra^{1,2}, Anupam Sahoo¹ & Srikanta Patra¹✉

Herein, we report a magnetically retrievable mixed-valent $\text{Fe}_3\text{O}_4@\text{SiO}_2/\text{Pd}^0/\text{Pd}^{\text{II}}$ NP (5) nanocomposite system for tandem Suzuki coupling/transfer hydrogenation reaction. The nanocomposite 5 was prepared first by making a layer of SiO_2 on Fe_3O_4 NP followed by deposition of Pd^0 and sorption of Pd^{II} ions successively onto the surface of $\text{Fe}_3\text{O}_4@\text{SiO}_2$ NP. The nanocomposite was characterized by powder XRD, electron microscopy (SEM-EDS and TEM-EDS) and XPS spectroscopy techniques. The mixed-valent $\text{Pd}^0/\text{Pd}^{\text{II}}$ present onto the surface of nanocomposite 5 was confirmed by XPS technique. Interestingly, the mixed-valent nanocomposite $\text{Fe}_3\text{O}_4@\text{SiO}_2/\text{Pd}^0/\text{Pd}^{\text{II}}$ NP (5) exhibited tandem Suzuki coupling/transfer hydrogenation reaction during the reaction of aryl bromide with aryl boronic acid (90% of C). The nanocomposite 5 displayed much better reactivity as compared to the monovalent $\text{Fe}_3\text{O}_4@\text{SiO}_2/\text{Pd}^0$ NP (3) (25% of C) and $\text{Fe}_3\text{O}_4@\text{SiO}_2/\text{Pd}^{\text{II}}$ NP (4) (15% of C) nanocomposites. Further, because of the presence of magnetic Fe_3O_4 , the nanocomposite displayed its facile separation from the reaction mixture and reused at least for five catalytic cycles.

The design and development of environmentally benign efficient catalytic systems which can conduct multiple mechanistically distinct reaction (tandem reaction) in one-pot is a fascinating area of contemporary research^{1,2}. Such catalytic systems offer a greener way by reducing reaction steps, cost of the process, and most importantly reduce the generation of waste during a reaction^{1,2}. The most common and successful strategy to conduct tandem reactions is to combine multiple mechanistically distinct catalytic centers in one-pot under a suitable reaction condition. A major disadvantage of this strategy is catalytic incompatibility which reduces tandem efficiency³⁻⁵. The alternative is to incorporate different catalytic units into a single molecular framework⁶⁻¹⁰ or integrate into a suitable solid matrix^{4,11-13}. In both cases, a well-defined ligand-framework is required to achieve desired tandem output. Adding two different metal centers into a single molecular framework/suitable solid matrix is challenging and cumbersome. Moreover, separation of catalysts after completion of the reaction and their reuse is also a concern.

Both Suzuki–Miyaura C–C coupling reaction¹⁴ and transfer hydrogenation reaction¹⁵⁻¹⁷ have become an indispensable tool in organic synthesis and pharmaceutical chemistry as they offer access of facile C–C bond formation and hydrogenation without use of hazardous hydrogen gas. A large number of efficient catalytic systems (both homogeneous and heterogeneous) have been developed for conducting C–C coupling reaction and transfer hydrogenation reaction. Many of the catalytic systems are used in industrial processes and are commercially available. There are many important biaryl organic motifs, crucial for the preparation of natural products and chiral pharmaceuticals, which requires both C–C coupling as well as transfer hydrogenation reaction steps^{4,11,12}. A catalyst system capable of conducting both mechanistically distinct C–C coupling reaction and transfer hydrogenation reactions in one-pot is highly appealing. Nevertheless, catalyst systems capable conducting tandem Suzuki coupling/transfer hydrogenation reaction are limited^{4,10-12}. In most of the cases, heterobimetallic systems (Pd–Ru) have been used as catalysts for conducting aforesaid tandem reaction^{6-9,18}. Interestingly, recently our group has observed that the tandem Suzuki coupling/transfer hydrogenation reaction can be conducted using bimetallic $\text{Pd}^{\text{I}}-\text{Pd}^{\text{II}}$ system efficiently.¹⁹ The palladium center in its zero-oxidation state (Pd^0) initiates the C–C

¹School of Basic Sciences, Indian Institute of Technology Bhubaneswar, Argul, Jatni, Odisha 752050, India. ²These authors contributed equally: Parminder Singh and Saumyaranjan Mishra. ✉email: srikanta@iitbbs.ac.in

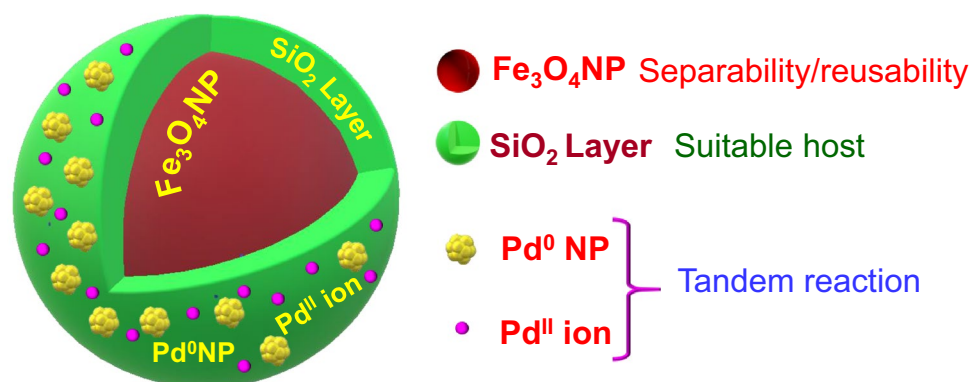


Figure 1. Magnetically retrievable $\text{Fe}_3\text{O}_4@\text{SiO}_2/\text{Pd}^0/\text{Pd}^{\text{II}}\text{NP}$ (5) nanocatalyst system and its advantages.

coupling reaction, whereas the palladium center in +2 oxidation state (Pd^{II}) carried out transfer hydrogenation reaction. It is to be noted that in all the cases, a well-defined ligand-framework is used to make the catalysts. It will be highly attractive if such kind of catalyst systems can be made without ligand-framework. Another interesting feature of a great catalytic system is its separability and reusability. This allows the catalyst to be separated and reused after catalytic conversion and thereby enhances the catalytic efficiency. Thus, designing a catalyst system without the use of ligand with facile separation ability is highly appealing.

With their high surface to volume ratio, interesting redox, optical, and catalytic properties, nanoparticles are attractive and become a fascinating tool for the development of tailor-made materials. The nanoparticles extend the easy incorporation of second nanoparticles onto the first one and also allow facile surface modification using different functionalities. This way, different interesting properties can easily be inserted into a single nanoparticle and thereby achieving materials with advanced features and desired properties. Considering this, several multimetallic nanoparticles systems have been developed and studied. However, the study of catalytic tandem reactivity is relatively less^{20–24}.

Utilizing the benefits of nanoparticles and advantages of one-pot multistep reactions, in the present contribution, we wish to demonstrate a magnetically retrievable mixed-valent multimetallic $\text{Fe}_3\text{O}_4@\text{SiO}_2/\text{Pd}^0/\text{Pd}^{\text{II}}\text{NP}$ (5) nanocatalytic system (Fig. 1) for efficient tandem Suzuki coupling/transfer hydrogenation reaction. $\text{Fe}_3\text{O}_4\text{NP}$ is used to insert magnetic property, and a layer of SiO_2 on $\text{Fe}_3\text{O}_4\text{NP}$ helps to host PdNP as well as Pd^{II} ions into the nanocomposite without use of any ligands. The nanocatalytic system 5 is characterized by SEM, TEM, powder XRD and XPS techniques. The catalytic reactivity of the synthesized nanocatalytic system is studied by conducting tandem Suzuki coupling/transfer hydrogenation reaction using aryl boronic acid and aryl bromide. Further, to compare the performance of the mixed-valent $\text{Fe}_3\text{O}_4@\text{SiO}_2/\text{Pd}^0/\text{Pd}^{\text{II}}\text{NP}$ (5) system to the monovalent $\text{Fe}_3\text{O}_4@\text{SiO}_2/\text{Pd}^0\text{NP}$ (3) and $\text{Fe}_3\text{O}_4@\text{SiO}_2/\text{Pd}^{\text{II}}\text{NP}$ (4) were also synthesized and their tandem reactivity was studied.

Results and discussion

The magnetic Fe_3O_4 nanoparticles were synthesized by following the procedure reported elsewhere²⁵. Briefly, a mixture of FeSO_4 and $\text{Fe}_2(\text{SO}_4)_3$ (1:1 mole ratio) in alkaline solution (pH = 10) was heated at 50 °C for 1 h to yield $\text{Fe}_3\text{O}_4\text{NP}$ (1). A layer of SiO_2 was incorporated over $\text{Fe}_3\text{O}_4\text{NP}$ to form $\text{Fe}_3\text{O}_4@\text{SiO}_2\text{NP}$ (2) by adding tetraethylorthosilicate (TEOS) to it and stirring for 18 h²⁵. Palladium nanoparticle was deposited onto the surface of $\text{Fe}_3\text{O}_4@\text{SiO}_2\text{NP}$ in situ by reducing $\text{K}_2[\text{PdCl}_4]$ using NaBH_4 at low temperature $\text{Fe}_3\text{O}_4@\text{SiO}_2/\text{Pd}^0\text{NP}$ (3)²⁶. Palladium ions (Pd^{II}) on the surface of $\text{Fe}_3\text{O}_4@\text{SiO}_2\text{NP}$ was sorbed by adding K_2PdCl_4 solution with stirring to yield $\text{Fe}_3\text{O}_4@\text{SiO}_2/\text{Pd}^{\text{II}}\text{NP}$ (4). Mixed-valent $\text{Fe}_3\text{O}_4@\text{SiO}_2/\text{Pd}^0/\text{Pd}^{\text{II}}\text{NP}$ (5) was achieved by mixing $\text{Fe}_3\text{O}_4@\text{SiO}_2/\text{Pd}^0\text{NP}$ and K_2PdCl_4 solution. All the nanoparticles were separated magnetically, followed by successive washing with triple distilled water and dried under oven for further use. A layout for the preparation of mixed-valent $\text{Fe}_3\text{O}_4@\text{SiO}_2/\text{Pd}^0/\text{Pd}^{\text{II}}\text{NP}$ (5) is shown in Scheme S1.

The crystalline nature of the nanoparticles was examined by powder X-ray diffraction (XRD) study. Figure S1 represents the powder XRD pattern of the nanoparticles. The powder XRD pattern of $\text{Fe}_3\text{O}_4\text{NP}$ (1) displayed peaks centered at 2θ values = 30.8, 36.3, 43.9, 54.3 (s), 57.9, 63.5 and 75 (s) which could be indexed as (220), (311), (400), (422) and (511) plane corresponding to cubic lattice of $\text{Fe}_3\text{O}_4\text{NP}$ (1)[JCPDS File No: 19-0629]^{27–30}. A broad band centered at $2\theta = 25^\circ$ along with the bands for $\text{Fe}_3\text{O}_4\text{NP}$ was observed while a layer of silica over Fe_3O_4 introduced $\text{Fe}_3\text{O}_4@\text{SiO}_2\text{NP}$ (2)²⁹. No significant change other than a new but very weak signal at $2\theta = 40.27^\circ$ for $\text{Fe}_3\text{O}_4@\text{SiO}_2/\text{Pd}^0\text{NP}$ (3) was observed while Pd^0 was deposited onto $\text{Fe}_3\text{O}_4@\text{SiO}_2\text{NP}$ ³¹. No change for $\text{Fe}_3\text{O}_4@\text{SiO}_2/\text{Pd}^0/\text{Pd}^{\text{II}}\text{NP}$ (4) was observed during deposition of Pd^{II} ion to $\text{Fe}_3\text{O}_4@\text{SiO}_2\text{NP}$. No additional peak was observed for $\text{Fe}_3\text{O}_4@\text{SiO}_2/\text{Pd}^0/\text{Pd}^{\text{II}}\text{NP}$ (5) during the deposition of Pd^{II} ion onto $\text{Fe}_3\text{O}_4@\text{SiO}_2/\text{Pd}^0\text{NP}$.

The surface morphology of the nanoparticles was investigated by Field Emission Scanning Electron Microscopy (FE-SEM) technique. The representative images are presented in Figures S2 and S3. It is observed from the images that the particles sizes are uniform and varying in the range ~ 30–45 nm. After deposition of Pd^0 onto $\text{Fe}_3\text{O}_4@\text{SiO}_2\text{NP}$ (2), the $\text{Fe}_3\text{O}_4@\text{SiO}_2/\text{Pd}^0\text{NP}$ (3) gets aggregated with particle size 38.4 ± 4.5 nm. No significant changes were observed in the morphology while the incorporation of Pd^{II} ions $\text{Fe}_3\text{O}_4@\text{SiO}_2/\text{Pd}^0\text{NP}$

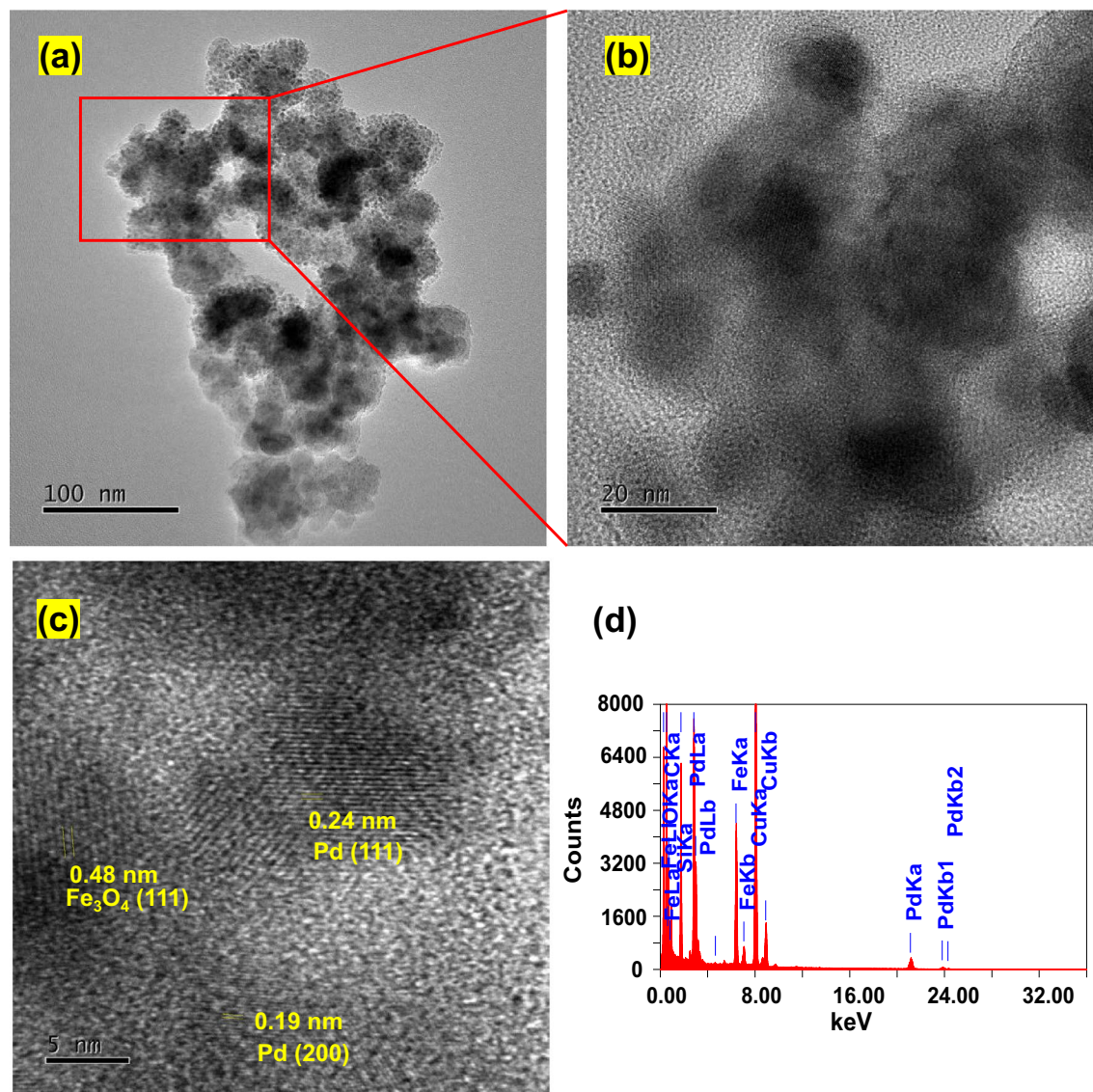


Figure 2. TEM and HRTEM images of $\text{Fe}_3\text{O}_4@/\text{SiO}_2/\text{Pd}^0/\text{Pd}^{\text{II}}$ NP (5) nanocomposite.

(4) (particle size 35.5 ± 5.6). The morphology of $\text{Fe}_3\text{O}_4@/\text{SiO}_2/\text{Pd}^0/\text{Pd}^{\text{II}}$ NP (5) (particle size 40.4 ± 5.4) remains the same after the introduction of Pd^{II} ions onto $\text{Fe}_3\text{O}_4@/\text{SiO}_2/\text{Pd}^0$ NP (3). The observed peaks corresponding to iron, silicon and palladium in the EDS spectra, indicating their presence in the nanocomposites (Figures S2 and S3). The elemental mapping of $\text{Fe}_3\text{O}_4@/\text{SiO}_2/\text{Pd}^0/\text{Pd}^{\text{II}}$ NP (5) further supports the presence of the elements in the nanocomposite (Figure S3).

The formation of $\text{Fe}_3\text{O}_4@/\text{SiO}_2/\text{Pd}^0/\text{Pd}^{\text{II}}$ NP (5) was further confirmed by high-resolution transmission images microscopy (HRTEM) (Fig. 2a,b). The EDS analysis of 5 shown the peaks corresponding to iron, palladium and silicon, which are in line with SEM analysis (*vide supra*) (Fig. 2d). The HRTEM image of the nanocomposite 5 has also shown the lattice fringes 0.48 nm for oxidized iron (020)³², and 0.19 nm for palladium (200)^{33,34} and 0.224 nm for palladium (111)^{34,35} which further confirms the presence of the elements (Fig. 2c).

To elucidate the surface composition and oxidation state of the elements present in the nanocomposite 5, X-ray photoelectron spectroscopy (XPS) study was conducted (Fig. 3). The XPS survey scan spectrum of 5 discloses the presence of iron, silicon, and palladium (Fig. 3a). The high resolution XPS spectra of 5 display peaks at 101.8 eV corresponding to Si^{2+} (Fig. 3c)³⁶, 710.26 eV and 723.85 eV corresponding to $2\text{p}_{3/2}$ and $2\text{p}_{1/2}$ of Fe^{2+} and Fe^{3+} (Fig. 3d)^{37,38}. The peaks at 334.78 eV and 340.16 eV; 337.73 eV and 342.85 eV correspond to $3\text{d}_{5/2}$ and $3\text{d}_{3/2}$ of metallic palladium (Pd^0) and oxidized palladium [Pd^{II} : PdO or $\text{Pd}(\text{OH})_2$] (Fig. 3b)^{26,31,33,39–46}. This confirms presence of mixed-valent palladium (Pd^0 and Pd^{II}) in nanocomposite 5.

It is well-known that both Pd^0 and Pd^{II} can conduct efficient Suzuki coupling reaction^{19,40,47–49}. Recent literatures also demonstrate that palladium (both Pd^0 and Pd^{II}) can catalyze transfer hydrogenation reaction^{19,50–57}. We, thus, presumed that the nanocatalyst $\text{Fe}_3\text{O}_4@/\text{SiO}_2/\text{Pd}^0/\text{Pd}^{\text{II}}$ NP (5) can conduct mechanically distinct Suzuki coupling and transfer hydrogenation reactions as it comprises palladium in both Pd^{II} as well as Pd^0 oxidation state. With this hypothesis, we attempted to conduct tandem Suzuki coupling/transfer hydrogenation reactions.

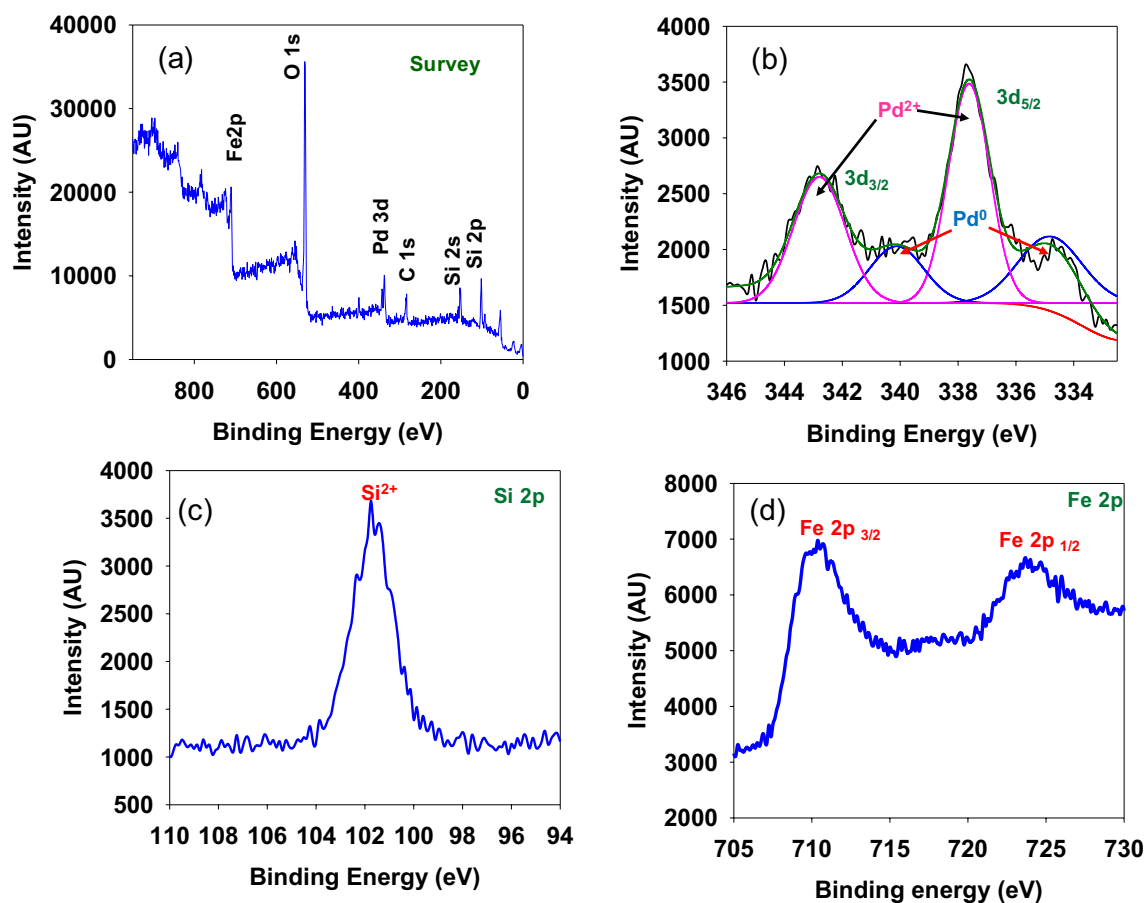


Figure 3. (a) XPS survey scan spectrum and high-resolution (b) Pd 3d_{5/2} and 3d_{3/2}, (c) Si 2p and (d) Fe 2p_{3/2} and 2p_{1/2} of Fe₃O₄@SiO₂/Pd⁰/Pd^{II}NP (5).

The tandem reaction was carried out using *p*-bromoacetophenone and phenylboronic acid in *i*PrOH as solvent and NaOH as base (Table 1). It was observed that the nanocatalyst 5 resulted in excellent yield of tandem product (entry 1, Table 1). The tandem reaction using nanocatalyst 5 was tested by varying solvents (Table 1). It was observed that the *i*PrOH is the best solvent for tandem reaction (entries 1, 5 and 6, Table 1). Further, the tandem reaction was found to be highly dependent on selection of base. The formation of tandem product C (90 %) was best during the use of NaOH as base (entry 1, Table 1). It was 85% under same reaction condition while KOH was used (entry 2, Table 1). The formation of tandem product (C) was significantly reduced (56%) when K^tOBu was used as base (entry 3, Table 1). Surprisingly, no tandem product (C) was formed when the base Cs₂CO₃ was used (entry 4, Table 1), however, the yield of coupling product (B) was appreciably high (93%) (entry 4, Table 1). This suggests that the use of bases like KOH and NaOH plays an important role to result in the formation of tandem product (C). Thus, the optimum reaction condition for the nanocatalyst 5 to achieve the best tandem efficiency is Catalyst/4-bromoacetophenone/PhB(OH)₂/NaOH 1mg/0.1 mmol/0.14 mmol/0.7 mmol, *i*PrOH 1 mL and reaction time 6 h (entry 1, Table 1). The tandem reaction using nanocatalyst 3 and 4 were also conducted. Both the nanocatalyst 3 and 4 under identical reaction condition resulted in much inferior yield of tandem product C (25% and 15%) as compared to the mixed-valent nanocatalyst 5 (entries 7 and 8, Table 1) leaving a major amount of hydrogenated product A (65% and 76%, respectively). This implies the importance of the presence of palladium in both (Pd^{II} and Pd⁰) oxidation states. It is also observed that pre-attainment of suitable oxidation states of metal atoms [Pd⁰ and Pd^{II}] for two mechanistically different reactions leads to much higher catalytic efficiency than that of monovalent [Pd⁰ or Pd^{II}] systems²⁷. Both the nanocatalyst Fe₃O₄NP (1) and Fe₃O₄@SiO₂NP (2) without any Pd^{II}/Pd⁰ were unable to yield the tandem product (A). However, the nanocatalyst 1 was found to act as a good transfer hydrogenation catalyst (Yield of A, 90%), whereas, the nanocatalyst 2 exhibited poor yield of A (30%) using excess of catalyst (5 mg in each cases) and longer reaction time 18 h (entry 11 and 12, Table 1).

Next, we conducted a time monitored reaction profile study of 4-bromoacetophenone and phenylboronic acid in the presence of NaOH in *i*PrOH at 85 °C using nanocatalyst 5 (Fig. 4). It appears from the reaction profile diagram that the Suzuki coupling reaction and transfer hydrogenation reaction occur simultaneously, and the rate of C–C coupling reaction is faster than the transfer hydrogenation reaction (Fig. 4). In fact, the transfer hydrogenation reaction follows an induction period of 15 min. This suggests that the C–C coupling reaction is more facile than the transfer hydrogenation reaction under this set of reaction condition. The reaction profile study further demonstrates the consecutive nature of mechanistically independent reactions, where reaction initiated with C–C coupling reaction between 4-bromoacetophenone and phenylboronic acid in step I, and subsequently,

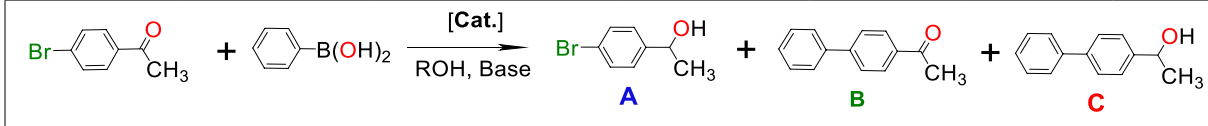
						
Entry	Cat.	ROH	Base	Yield ^a		
				A	B	C
1	5	<i>i</i> PrOH	NaOH	0	Trace	90
2	5	<i>i</i> PrOH	KOH	Trace	0	85
3	5	<i>i</i> PrOH	KO ^t Bu	20*	10	56*
4	5	<i>i</i> PrOH	Cs ₂ CO ₃	0	93	0
5	5	<i>n</i> -PrOH	NaOH	0	45	10
6	5	PhCH ₂ OH	NaOH	0	Trace	0
7	5 + Hg	<i>i</i> PrOH	NaOH	0	0	15
8 ^b	3+4	<i>i</i> PrOH	NaOH	0	0	75
9 ^c	3	<i>i</i> PrOH	NaOH	65	0	25*
10 ^c	4	<i>i</i> PrOH	NaOH	76	0	15*
11 ^{c,d}	2	<i>i</i> PrOH	NaOH	30	0	0
12 ^{c,d}	1	<i>i</i> PrOH	NaOH	90	0	0

Table 1. Tandem Suzuki coupling/transfer hydrogenation of 4-bromoacetophenone and phenylboronic acid. Reaction condition: Catalyst/4-bromoacetophenone/ PhB(OH)₂/base 1.0 mg/0.1 mmol/0.14 mmol/0.7 mmol, ROH 1.0 mL, reaction temperature 85 °C, reaction time 6 h. ^aIsolated yields (¹H NMR Yield). ^bAmount of 3 and 4 is 1.0 mg each. ^cReaction time 18 h. ^dCatalyst amount 5.0 mg.

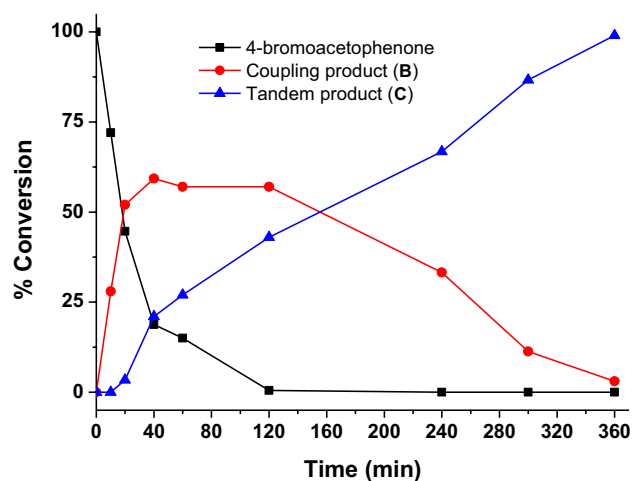


Figure 4. Reaction profile diagram for the tandem Suzuki coupling/transfer hydrogenation reaction catalyzed by nanocomposite 5.

the coupling product (B) gets hydrogenated to yield the tandem product (C) in step II. Palladium mediated C–C coupling reaction or transfer hydrogenation is known; however, tandem reaction utilizing mixed-valent palladium centers (Pd⁰/Pd^{II}) is rare^{27,56,58}. Thus, the present ligand-free mixed-valent Pd⁰/Pd^{II} nanocatalyst system 5 is an important addition to this tandem catalysis.

Further, the reversibility of the catalytic tandem Suzuki-Miyaura C–C coupling/transfer hydrogenation reaction was monitored using ¹H NMR spectroscopy by conducting the reverse reaction using the tandem product 1-([1,1'-biphenyl]-4-yl)ethan-1-ol (C) under the identical reaction condition. No trace of the progress of the reaction was observed in ¹H NMR spectrum, indicating irreversible nature of the catalytic cycle.

Based on this experimental finding and literature data a plausible tandem reaction mechanism is proposed (Fig. 5)^{59–63}. The tandem reaction is initiated with the formation of Suzuki-Miyaura C–C coupling reaction product (B) between 4-bromoacetophenone and phenylboronic acid at Pd⁰ center (catalytic cycle I). The formed coupling product then enters into the catalytic cycle II, where it gets transfer hydrogenated to tandem product (C) catalyzed by Pd^{II} center in the presence of *i*PrOH as hydrogen donor.

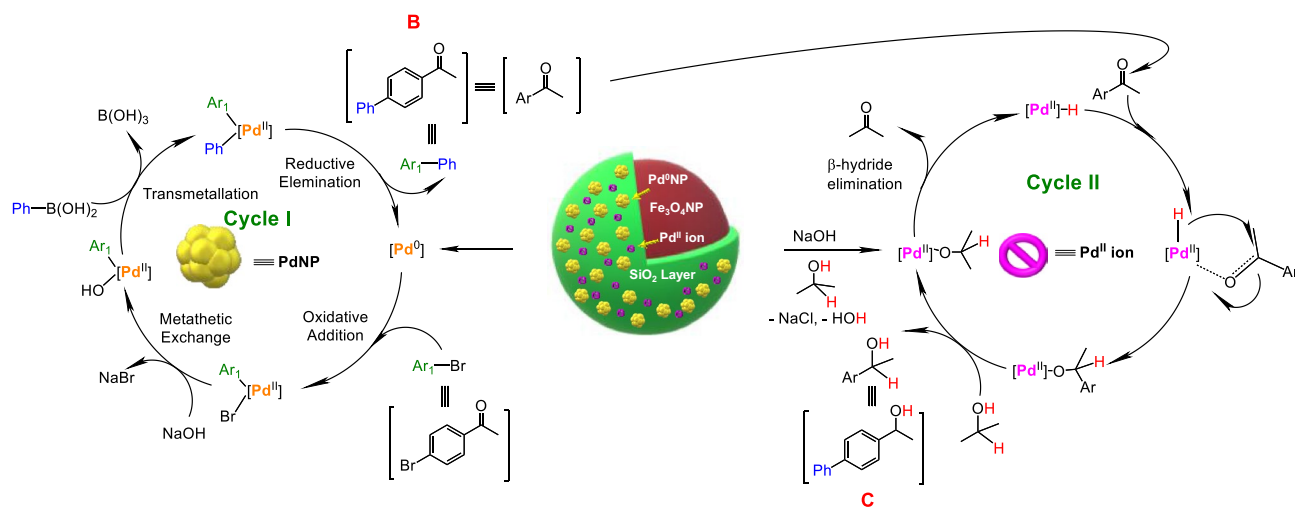


Figure 5. Plausible mechanism for tandem Suzuki coupling/transfer hydrogenation reaction catalysed by $\text{Fe}_3\text{O}_4@/\text{SiO}_2/\text{Pd}^0/\text{Pd}^{\text{II}}\text{NP}$ (**5**) nanocomposite^{59–63}.

Next, we extended our study to check the generality of the tandem Suzuki coupling/transfer hydrogenation reaction. The tandem reaction was conducted using different boronic acids of varying substituents (Table 2). In all the cases moderate to good yield of tandem product was registered. This suggests that the present nanocatalyst **5** has a good tolerance against various substrates. Further, the nature of substituents and their position in both boronic acid and haloarylketone are found to have a significant influence on the formation of tandem products.

Next, we performed mercury drop test to check the heterogeneity of the catalyst **5**^{6,64,65}. The yield of tandem product **C** reduced significantly to 15% (entry 7, Table 1) upon addition of metallic mercury during the course of reaction. This suggests the heterogeneous nature of the nanocatalyst **5**. Further, to check the heterogeneity and leaching of palladium to the solution, hot filtration study was performed by following the reported procedure⁶⁶. The filtrate did not show any catalytic activity under the optimized reaction condition. This further suggests that there is no leaching of the catalyst and the catalysis is heterogeneous in nature. Nevertheless, leaching of a small fraction of palladium from the nanocomposite surface to the solution may not be ruled out as there is formation of small amount of tandem product (**C**) during mercury poisoning test (entry 7, Table 1).

Another interesting feature of the present mixed-valent nanocatalyst $\text{Fe}_3\text{O}_4@/\text{SiO}_2/\text{Pd}^0/\text{Pd}^{\text{II}}\text{NP}$ (**5**) is its separability and reusability from the solution as it consists of magnetic Fe_3O_4 core. The nanocatalyst **5** exhibited its facile separation ability from aqueous solution by using an external magnet during its preparation. To check the separability and reusability, the nanocatalyst **5** was magnetically retrieved from the reaction mixture after completion of the reaction. The magnetically separated nanocatalyst **5** was washed thoroughly with *i*PrOH, dried, and reused for the tandem reaction. Interestingly, the tandem reactivity of nanocatalyst **5** did not change significantly, even after 5 cycles (Fig. 6). This demonstrates the efficient recyclability and reusability of nanocatalyst **5**, which is a desirable criterion for a good catalyst. Catalyst system exhibiting good tandem efficacy as well as excellent separation ability, and reusability are relatively rare. Thus, the present mixed-valent nanocatalyst **5** is an important example of tandem catalysis.

Conclusions

In conclusion, we have developed a magnetically retrievable efficient mixed-valent nanocatalyst $\text{Fe}_3\text{O}_4@/\text{SiO}_2/\text{Pd}^0/\text{Pd}^{\text{II}}\text{NP}$ (**5**). The nanocatalyst was characterized by FE-SEM-EDS, TEM, powder XRD techniques. The mixed-valent palladium ($\text{Pd}^0/\text{Pd}^{\text{II}}$) was confirmed by XPS analysis. Unlike mono-valent $\text{Fe}_3\text{O}_4@/\text{SiO}_2/\text{Pd}^0\text{NP}$ (**3**) and $\text{Fe}_3\text{O}_4@/\text{SiO}_2/\text{Pd}^{\text{II}}\text{NP}$ (**4**), the mixed-valent $\text{Fe}_3\text{O}_4@/\text{SiO}_2/\text{Pd}^0/\text{Pd}^{\text{II}}\text{NP}$ (**5**) nanocatalyst exhibits excellent tandem Suzuki coupling/transfer hydrogenation reactivity. The mixed-valent nanocatalyst **5** also offers facile magnetic separation and its repeated use for several cycles. A catalyst exhibiting tandem reactivity along with facile separation ability is rare. Thus, we envision that the present ligand-free mixed-valent nanocatalyst system **5** is an important example that will be useful for the communities working in the area of tandem catalysis. conclusions should come in this section at the end of the article, before the acknowledgements.

Experimental

Materials and methods. All chemicals were purchased from commercial sources and used as received. All glassware was cleaned using aqua regia, thoroughly washed with double distilled water, and rinsed with copious amount triple distilled water and dried in the oven. All reactions were carried out under an inert atmospheric condition using standard Schlenk techniques under the dinitrogen atmosphere unless and otherwise stated.

Instrumentation. ^1H and ^{13}C NMR spectra were recorded using Bruker 400 NMR spectrometer using CDCl_3 as solvent. FE-SEM images and EDS analyses were recorded using Zeiss Merlin compact Microscope and Oxford instruments, respectively by drop casting the nanoparticles sample on carbon tape. HRTEM images were

Entry	Ar-Br	Ar-B(OH) ₂	Product	Yield ^a
1				90
2				93
3				78
4				77
5				83
6				72
7				86
8				76

Table 2. Tandem Suzuki coupling/transfer hydrogenation of 4-bromoacetophenone. Reaction condition: Catalyst/4-bromoacetophenone/Ar-B(OH)₂/NaOH 1 mg/0.1mmol/0.14 mmol/0.7 mmol, ⁱPrOH 1 mL, reaction temperature 85 °C, reaction time 6 h. ^aIsolated yields.

acquired using JEOL JEM 2100 electron microscope. Powder XRD analyses were carried out using a Bruker D8 Advance Diffractometer (Bruker AXS) with Cu K_α radiation ($\lambda = 1.54 \text{ \AA}$) over a 2θ range of 10° – 110° with a scanning rate of $40^\circ/\text{min}$. The samples for powder XRD was prepared by making a thin film of nanocomposites on glass slide.

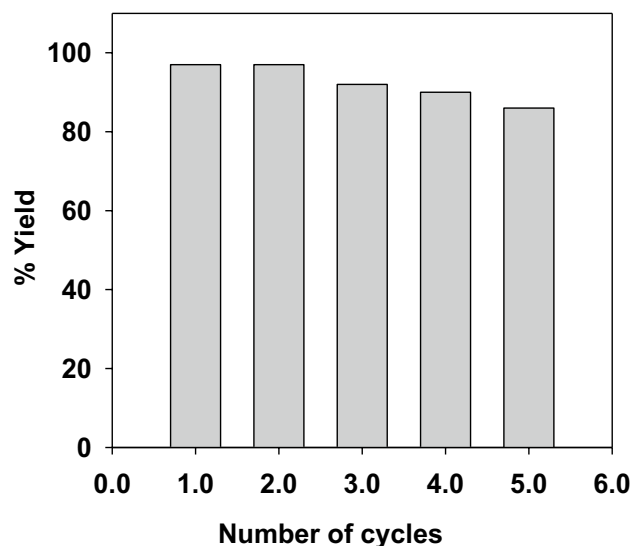


Figure 6. Reusability of $\text{Fe}_3\text{O}_4@SiO_2/Pd^0/Pd^{II}NP$ (5) nanocatalyst towards tandem Suzuki coupling/transfer hydrogenation reaction.

Synthesis of Fe_3O_4 NP (1). The Fe_3O_4 nanoparticles was prepared by following the reported procedure²⁵. Briefly, $\text{FeSO}_4 \cdot 7\text{H}_2\text{O}$ (278 mg, 1 mmol) and $\text{Fe}_2(\text{SO}_4)_3$ (400 mg, 1 mmol) were dissolved in 30 mL of water (3:1). The pH of the solution was adjusted to 10.0 by adding a solution of NH_4OH (25%) with stirring. The reaction mixture was then heated at 60°C for 1 h with constant stirring to yield Fe_3O_4NP (1). The reaction mixture was cooled to room temperature for further use.

Synthesis of $\text{Fe}_3\text{O}_4@SiO_2$ NP (2). The $\text{Fe}_3\text{O}_4@SiO_2$ nanoparticles was also prepared by following the reported procedure²⁵. To the solution of in-situ generated Fe_3O_4NP (1) at room temperature, tetraethylorthosilicate (TEOS) (1 mL, 4.48 mmol) was added with vigorous stirring. The stirring was continued for 18 h at room temperature. The formed $\text{Fe}_3\text{O}_4@SiO_2NP$ (2) was magnetically retrieved, washed several times with water and dried for further use (weight 500 mg).

Synthesis of $\text{Fe}_3\text{O}_4@SiO_2/Pd^0$ NP (3). To 30 mL aqueous suspension of $\text{Fe}_3\text{O}_4@SiO_2NP$ (2), an aqueous solution of $\text{K}_2[\text{PdCl}_4]$ (50 mg, 0.15 mmol) was added with continuous stirring. The stirring was continued for 6 h and cooled it in ice bath. To this cold solution, an aqueous solution of NaBH_4 (50 mg, 1.32 mmol) was added with stirring. The stirring was continued for an additional 12 h. The formed magnetic $\text{Fe}_3\text{O}_4@SiO_2/Pd^0NP$ (3) was then separated using an external magnet and washed several times with distilled water followed by ethanol and dried under vacuum and used for further studies.

Synthesis of $\text{Fe}_3\text{O}_4@SiO_2/Pd^{II}NP$ (4). To the aqueous solution (pH 10) of $\text{Fe}_3\text{O}_4@SiO_2NP$ (2), an aqueous solution of $\text{K}_2[\text{PdCl}_4]$ (50 mg, 0.15 mmol) was added with continuous stirring. The stirring was continued for 18 h. It was then washed several times with distilled water followed by ethanol and dried under vacuum to yield $\text{Fe}_3\text{O}_4@SiO_2/Pd^{II}NP$ (4).

Synthesis of $\text{Fe}_3\text{O}_4@SiO_2/Pd^0/Pd^{II}NP$ (5). The $\text{Fe}_3\text{O}_4@SiO_2/Pd^0NP$ (3) was suspended in 30 mL distilled water, and 4 mL of ammonia solution was added to it to reach pH 10.0. To this solution, 50 mg (0.15 mmol) of $\text{K}_2[\text{PdCl}_4]$ was added and stirred for 18 h. The obtained nanoparticles was washed several times with distilled water followed by ethanol and dried under vacuum to yield $\text{Fe}_3\text{O}_4@SiO_2/Pd^0/Pd^{II}$ (5) nanocomposite.

Study of catalytic activity. In a 10 mL Schlenk tube 0.1 mmol of 4-bromoacetophenon and 0.14 mmol of phenylboronic acid, 0.7 mmol of NaOH and 1 mg of catalyst were taken. The reaction vessel was degassed and filled with dinitrogen by using standard Schlenk techniques. To this reaction mixture, 1 mL dry $^i\text{PrOH}$ was added. The dinitrogen environment of the reaction mixture was maintained by using a balloon filled with nitrogen gas. The reaction mixture was then heated at reflux for 6 h with continuous stirring in a preheated (85°C) oil bath. The reaction was quenched by adding 4 mL dichloromethane (DCM). The crude products were then charged in a silica gel column. The pure products were isolated either by column chromatography or preparatory thin layered chromatography by using 90% hexane and 10% ethyl acetate as eluent. The compounds were dried under vacuum, and isolated yields were calculated. ^1H NMR and ^{13}C NMR spectra of the dried products were recorded.

The identical reaction condition as above was maintained for plotting the reaction profile diagram. The reactions were quenched at different time intervals using DCM. Flash chromatography was carried out to remove the

base and catalyst from the reaction mixture. The reaction mixture was then dried at reduced pressure. The composition of products in the reaction mixture at different time intervals was calculated using ^1H NMR spectroscopy by comparing the peak intensities of the compounds with the peak intensity of mesitylene (internal standard).

Received: 24 July 2020; Accepted: 28 February 2021

Published online: 29 April 2021

References

- Lee, J. M., Na, Y., Han, H. & Chang, S. Cooperative multi-catalyst systems for one-pot organic transformations. *Chem. Soc. Rev.* **33**, 302–312 (2004).
- Wasilke, J.-C., Obrey, S. J., Tom Baker, R. & Bazan, G. C. Concurrent tandem catalysis. *Chem. Rev.* **105**, 1001–1020 (2005).
- Lohr, T. L. & Marks, T. J. Orthogonal tandem catalysis. *Nat. Chem.* **7**, 477–482 (2015).
- Shu, X., Jin, R., Zhao, Z., Cheng, T. & Liu, G. An integrated immobilization strategy manipulates dual active centers to boost enantioselective tandem reactions. *Chem. Commun.* **54**, 13244–13247 (2018).
- Blaser, H. U. & Federsel, H.-J. *Asymmetric Catalysis on Industrial Scale: Challenges, Approaches and Solutions* (Wiley-VCH, 2010).
- Dehury, N., Tripathy, S. K., Sahoo, A., Maity, N. & Patra, S. Facile tandem Suzuki coupling/transfer hydrogenation reaction with a bis-heteroscorpionate Pd–Ru complex. *Dalton Trans.* **43**, 16597–16600 (2014).
- Zanardi, A., Mata, J. A. & Peris, E. Well-defined Ir/Pd complexes with a triazolyl-diylidene bridge as catalysts for multiple tandem reactions. *J. Am. Chem. Soc.* **131**, 14531–14537 (2009).
- Mata, J. A., Hahn, F. E. & Peris, E. Heterometallic complexes, tandem catalysis and catalytic cooperativity. *Chem. Sci.* **5**, 1723–1732 (2014).
- Pezük, L. G., Şen, B., Hahn, F. E. & Türkmen, H. Heterobimetallic complexes bridged by imidazol[4,5-f][1,10]-phenanthroline-2-ylidene: Synthesis and catalytic activity in tandem reactions. *Organometallics* **38**, 593–601 (2019).
- Bitzer, M. J., Kühn, F. E. & Baratta, W. Tandem Suzuki–Miyaura/transfer hydrogenation reaction catalyzed by a Pd–Ru complex bearing an anionic dicarbene. *J. Catal.* **338**, 222–226 (2016).
- Meng, J. *et al.* Switchable catalysts used to control Suzuki cross-coupling and aza-michael addition/asymmetric transfer hydrogenation cascade reactions. *ACS Catal.* **9**, 8693–8701 (2019).
- Zhang, G. *et al.* Multiple functionalized hyperbranched polyethoxysiloxane promotes Suzuki coupling asymmetric transfer hydrogenation one-pot enantioselective organic transformations. *ChemCatChem* **10**, 1882–1888 (2018).
- Mahato, S. K. *et al.* Fe-polyaniline composite nanofiber catalyst for chemoselective hydrolysis of oxime. *J. Colloid Interface Sci.* **513**, 592–601 (2018).
- Miyaura, N., Yamada, K. & Suzuki, A. A new stereospecific cross-coupling by the palladium-catalyzed reaction of 1-alkenylboranes with 1-alkenyl or 1-alkynyl halides. *Tetrahedron Lett.* **20**, 3437–3440 (1979).
- Knoevenagel, E. & Bergdolt, B. Ueber das Verhalten des Δ 2.5-Dihydroterephthalsäuredimethylesters bei höheren Temperaturen und in Gegenwart von Palladiummohr. *Berichte der Dtsch. Chem. Gesellschaft* **36**, 2857–2860 (1903).
- Wieland, H. Über Hydrierung und Dehydrierung. *Berichte der Dtsch. Chem. Gesellschaft* **45**, 484–493 (1912).
- Braude, E. A. & Linstead, R. P. Hydrogen transfer. Part I. Introductory survey. *J. Chem. Soc.* <https://doi.org/10.1039/JR9540003544> (1954).
- Majumder, A., Naskar, R., Roy, P. & Maity, R. Homo- and heterobimetallic complexes bearing NHC ligands: Applications in α -arylation of amide, Suzuki–Miyaura coupling reactions, and tandem catalysis. *Eur. J. Inorg. Chem.* <https://doi.org/10.1002/ejic.201801570> (2019).
- Dehury, N., Maity, N., Tripathy, S. K., Basset, J.-M. & Patra, S. Dinuclear tetrapyrazolyl palladium complexes exhibiting facile tandem transfer hydrogenation/Suzuki coupling reaction of fluoroarylketone. *ACS Catal.* **6**, 5535–5540 (2016).
- Kaur, M., Pramanik, S., Kumar, M. & Bhalla, V. Polythiophene-encapsulated bimetallic Au–Fe₃O₄ nano-hybrid materials: A potential tandem photocatalytic system for nondirected C(sp²)-H activation for the synthesis of quinoline carboxylates. *ACS Catal.* **7**, 2007–2021 (2017).
- Woo, H. *et al.* A new hybrid nanocatalyst based on Cu-doped Pd–Fe₃O₄ for tandem synthesis of 2-phenylbenzofurans. *J. Mater. Chem. A* **3**, 20992–20998 (2015).
- Jagadeesan, D. Multifunctional nanocatalysts for tandem reactions: A leap toward sustainability. *Appl. Catal. A* **511**, 59–77 (2016).
- Miyamura, H. & Kobayashi, S. Tandem oxidative processes catalyzed by polymer-incarcerated multimetallic nanoclusters with molecular oxygen. *Acc. Chem. Res.* **47**, 1054–1066 (2014).
- Shiraishi, Y., Fujiwara, K., Sugano, Y., Ichikawa, S. & Hirai, T. N-monoalkylation of amines with alcohols by tandem photocatalytic and catalytic reactions on TiO₂ loaded with Pd nanoparticles. *ACS Catal.* **3**, 312–320 (2013).
- Nasir Baig, R. B. & Varma, R. S. Magnetic silica-supported ruthenium nanoparticles: An efficient catalyst for transfer hydrogenation of carbonyl compounds. *ACS Sustain. Chem. Eng.* **12**, 805–809. <https://doi.org/10.1021/sc400032k> (2013).
- Bhardwaj, M., Sharma, H., Paul, S. & Clark, J. H. Fe₃O₄@SiO₂/EDAC–Pd(0) as a novel and efficient inorganic/organic magnetic composite: Sustainable catalyst for the benzylic C–H bond oxidation and reductive amination under mild conditions. *New J. Chem.* **40**, 4952–4961 (2016).
- Arroniz, C., Chaubet, G. & Anderson, E. A. Dual oxidation state tandem catalysis in the palladium-catalyzed isomerization of alkenyl epoxides to furans. *ACS Catal.* **8**, 8290–8295 (2018).
- Jiang, Y., Cai, W., Tu, W. & Zhu, M. Facile cross-link method to synthesize magnetic Fe₃O₄@SiO₂-chitosan with high adsorption capacity toward hexavalent chromium. *J. Chem. Eng. Data* **64**, 226–233 (2019).
- Baby, T. T. & Ramaprabhu, S. SiO₂ coated Fe₃O₄ magnetic nanoparticle dispersed multiwalled carbon nanotubes based amperometric glucose biosensor. *Talanta* **80**, 2016–2022 (2010).
- Prilepskii, A. Y. *et al.* Urokinase-conjugated magnetite nanoparticles as a promising drug delivery system for targeted thrombolysis: Synthesis and preclinical evaluation. *ACS Appl. Mater. Interfaces* **10**, 36764–36775 (2018).
- Pino, N. *et al.* Structure, activity, and selectivity of bimetallic Pd–Fe/SiO₂ and Pd–Fe/γ-Al₂O₃ catalysts for the conversion of furfural. *J. Catal.* **350**, 30–40 (2017).
- Hu, H. *et al.* Unique role of ionic liquid in microwave-assisted synthesis of monodisperse magnetite nanoparticles. *Chem. Commun.* **46**, 3866–3868 (2010).
- Zhao, J. *et al.* A hierarchical heterostructure based on Pd nanoparticles/layered double hydroxide nanowalls for enhanced ethanol electrooxidation. *J. Mater. Chem. A* **1**, 5840–5846 (2013).
- Deng, Q. F., Zhang, Z. F., Cui, F. J. & Jia, L. H. Highly dispersed Pd–MnOx nanoparticles supported on graphitic carbon nitride for hydrogen generation from formic acid-formate mixtures. *Int. J. Hydrog. Energy* **42**, 14865–14871 (2017).
- Liu, M. *et al.* The green synthesis of Pd(O)/Pd anchored on hierarchical ZnO microflowers with a synthetic effect for the efficient catalytic reduction of 4-nitrophenol. *New J. Chem.* **44**, 7035–7041 (2020).
- Oluwasina, O. O., Lajide, L. & Owolabi, B. Microcrystalline cellulose from plant wastes through sodium hydroxide-anthraquinone-ethanol pulping. *BioResources* **9**, 3554–3570 (2014).

37. Wang, L. *et al.* Fabrication of hierarchical graphene@Fe₃O₄@SiO₂@polyaniline quaternary composite and its improved electrochemical performance. *J. Alloys Compd.* **634**, 232–238 (2015).
38. Lo, C. K., Xiao, D. & Choi, M. M. F. Homocysteine-protected gold-coated magnetic nanoparticles: Synthesis and characterisation. *J. Mater. Chem.* **17**, 2418–2427 (2007).
39. Sá, S. *et al.* Magnetically recyclable magnetite–palladium (Nanocat-Fe–Pd) nanocatalyst for the Buchwald–Hartwig reaction. *Green Chem.* **16**, 3494–3500 (2014).
40. Veisi, H., Najafi, S. & Hemmati, S. Pd(II)/Pd(0) anchored to magnetic nanoparticles (Fe₃O₄) modified with biguanidine-chitosan polymer as a novel nanocatalyst for Suzuki–Miyaura coupling reactions. *Int. J. Biol. Macromol.* **113**, 186–194 (2018).
41. Tang, Y. *et al.* Effect of Fe state on electrocatalytic activity of Pd–Fe/C catalyst for oxygen reduction. *Appl. Surf. Sci.* **256**, 4196–4200 (2010).
42. Li, T. *et al.* Scalable synthesis of Ag networks with optimized sub-monolayer Au–Pd nanoparticle covering for highly enhanced SERS detection and catalysis. *Sci. Rep.* **6**, 1–11 (2016).
43. Celebi, M., Yurderi, M., Bulut, A., Kaya, M. & Zahmakiran, M. Palladium nanoparticles supported on amine-functionalized SiO₂ for the catalytic hexavalent chromium reduction. *Appl. Catal. B Environ.* **180**, 53–64 (2016).
44. Wang, Q. *et al.* Hierarchical structure based on Pd(Au) nanoparticles grafted onto magnetite cores and double layered shells: Enhanced activity for catalytic applications. *J. Mater. Chem. A* **1**, 12732–12741 (2013).
45. Shaikh, M. N. Pd nanoparticles on green support as dip-catalyst: A facile transfer hydrogenation of olefins and N-heteroarenes in water. *RSC Adv.* **9**, 28199–28206 (2019).
46. Marx, S. & Baiker, A. Beneficial interaction of gold and palladium in bimetallic catalysts for the selective oxidation of benzyl alcohol. *J. Phys. Chem. C* **113**, 6191–6201 (2009).
47. Paul, S., Islam, M. M. & Islam, S. M. Suzuki–Miyaura reaction by heterogeneously supported Pd in water: Recent studies. *RSC Adv.* **5**, 42193–42221 (2015).
48. Varadwaj, G. B. B., Rana, S. & Parida, K. Pd(0) nanoparticles supported organofunctionalized clay driving C–C coupling reactions under benign conditions through a Pd(0)/Pd(II) redox interplay. *J. Phys. Chem. C* **118**, 1640–1651 (2014).
49. Zhao, Y. *et al.* Fabrication of Te@Pd core–shell hybrids for efficient C–C coupling reactions. *J. Phys. Chem. C* **116**, 7416–7420 (2012).
50. Scholz, D., Aellig, C. & Hermans, I. Catalytic transfer hydrogenation/hydrogenolysis for reductive upgrading of furfural and 5-(hydroxymethyl)furfural. *ChemSusChem* **7**, 268–275 (2014).
51. Hauwert, P., Boerleider, R., Warsink, S., Weigand, J. J. & Elsevier, C. J. Mechanism of Pd(NHC)-catalyzed transfer hydrogenation of alkynes. *J. Am. Chem. Soc.* **132**, 16900–16910 (2010).
52. Németh, J., Kiss, Á. & Hell, Z. Palladium-catalyzed transfer hydrogenation of nitrobenzenes: Investigation of the selectivity. *React. Kinet. Mech. Catal.* **111**, 115–121 (2014).
53. Cummings, S. P., Le, T. N., Fernandez, G. E., Quiambao, L. G. & Stokes, B. J. Tetrahydroxydiboron-mediated palladium-catalyzed transfer hydrogenation and deuteration of alkenes and alkynes using water as the stoichiometric H or D atom donor. *J. Am. Chem. Soc.* **138**, 6107–6110 (2016).
54. Mandal, P. K. & McMurray, J. S. Pd–C-induced catalytic transfer hydrogenation with triethylsilane. *J. Org. Chem.* **72**, 6599–6601 (2007).
55. Ciszek, B. & Fleischer, I. Homogeneous palladium-catalyzed transfer hydrogenolysis of benzylic alcohols using formic acid as reductant. *Chem. Eur. J.* **24**, 12259–12263 (2018).
56. Nie, R. *et al.* Transfer hydrogenation of bio-fuel with formic acid over biomass-derived N-doped carbon supported acid-resistant Pd catalyst. *Catal. Sci. Technol.* **7**, 627–634 (2017).
57. Mahato, S. K., Ul Islam, R., Acharya, C., Witcomb, M. J. & Mallick, K. Polymer-stabilized palladium nanoparticles for the chemoselective transfer hydrogenation of α , β -unsaturated carbonyls: Single-step bottom-up approach. *ChemCatChem* **6**, 1419–1426 (2014).
58. Cui, X. *et al.* Pd-doped Ni nanoparticle-modified N-doped carbon nanocatalyst with high Pd atom utilization for the transfer hydrogenation of nitroarenes. *Green Chem.* **20**, 1121–1130 (2018).
59. Balanta, A., Godard, C. & Claver, C. Pd nanoparticles for C–C coupling reactions. *Chem. Soc. Rev.* **40**, 4973–4985 (2011).
60. Zhang, B. & Yan, N. Towards rational design of nanoparticle catalysis in ionic liquids. *Catalysts* **3**, 543–562 (2013).
61. Bej, A., Ghosh, K., Sarkar, A. & Knight, D. W. Palladium nanoparticles in the catalysis of coupling reactions. *RSC Adv.* **6**, 11446–11453 (2016).
62. Ellis, P. J., Fairlamb, I. J. S., Hackett, S. F. J., Wilson, K. & Lee, A. F. Evidence for the surface-catalyzed Suzuki–Miyaura reaction over palladium nanoparticles: An operando XAS study. *Angew. Chem.* **122**, 1864–1868 (2010).
63. Pentsak, E. O. & Ananikov, V. P. Pseudo-solid-state Suzuki–Miyaura reaction and the role of water formed by dehydration of arylboronic acids. *Eur. J. Org. Chem.* <https://doi.org/10.1002/ejoc.201900410> (2019).
64. Dehury, N., Maity, N., Tripathy, S., Basset, J.-M. & Patra, S. Dinuclear tetrapyrzoyl palladium complexes exhibiting facile tandem transfer hydrogenation/Suzuki coupling reaction of fluoroarylketone. *ACS Catal.* **6**, 5535–5540 (2016).
65. Depasquale, J., Kumar, M., Zeller, M. & Papish, E. T. Variations on an NHC theme: Which features enhance catalytic transfer hydrogenation with ruthenium complexes? *Organometallics* **32**, 966–979 (2013).
66. Ji, Y., Jain, S. & Davis, R. J. Investigation of Pd leaching from supported Pd catalysts during the Heck reaction. *J. Phys. Chem. B* **109**, 17232–17238 (2005).

Acknowledgements

The authors would like to acknowledge the Council of Scientific and Industrial Research (File No. 01(2932)/18/EMR-II) and the Science and Engineering Research Board (SERB) (File No. CRG/2018/000173 dated 28/02/2019) for financial supports. The authors would like to dedicate this article to Professor Wolfgang Kaim on his 70th birthday.

Author contributions

P.S.: Conducted partial experiments and carried out the partial characterization, data analysis. S.M.: Conducted partial experiments and carried out the partial characterization, data analysis. A.S.: Assist in conducting experiments and conducted some of the characterizations and figure preparation and data analysis. Dr. S.P.: Manuscript writing and figure preparation, data analysis, etc. All the authors reviewed the manuscript

Competing interests

The authors declare no competing interests.

Additional information

Supplementary Information The online version contains supplementary material available at <https://doi.org/10.1038/s41598-021-88528-6>.

Correspondence and requests for materials should be addressed to S.P.

Reprints and permissions information is available at www.nature.com/reprints.

Publisher's note Springer Nature remains neutral with regard to jurisdictional claims in published maps and institutional affiliations.



Open Access This article is licensed under a Creative Commons Attribution 4.0 International License, which permits use, sharing, adaptation, distribution and reproduction in any medium or format, as long as you give appropriate credit to the original author(s) and the source, provide a link to the Creative Commons licence, and indicate if changes were made. The images or other third party material in this article are included in the article's Creative Commons licence, unless indicated otherwise in a credit line to the material. If material is not included in the article's Creative Commons licence and your intended use is not permitted by statutory regulation or exceeds the permitted use, you will need to obtain permission directly from the copyright holder. To view a copy of this licence, visit <http://creativecommons.org/licenses/by/4.0/>.

© The Author(s) 2021